

Modeling of Wave Dispersion Using Continuous Wavelet Transforms II: Wavelet-based Frequency-velocity Analysis

M. KULESH,¹ M. HOLSCHNEIDER,¹ M. OHRNBERGER,² and E. LÜCK²

Abstract—In this paper, we show how to estimate the phase velocities of multi-mode signals as present in 2-D shallow seismic surveys along a seismic line with the help of a method that is based on the deformation of the wavelet spectra of the seismic traces. In analogy with frequency-wavenumber (f - k) analysis, we perform “frequency-velocity” analysis using the correlations between phases of the wavelet spectra. Our method has two tuning parameters — the parameter of an analyzing wavelet and the parameter of a threshold operation. Numerical and experimental examples are presented to illustrate how the method accurately extracts the phase velocity from single- and multi-mode signals.

Key words: Continuous wavelet transform, multimode signal, dispersion, phase deformation.

1. Introduction

In this paper, we continue the series of studies dedicated to the modeling of dispersed and attenuated wave propagation with the help of the continuous wavelet transform. We consider a 2-D shallow seismic survey (stations along a line) and assume a single source and a geometrical configuration where the source and the receiver stations are aligned.

In this situation we have shown in KULESH *et al.* (2005), how the wavelet transform of the source and the propagated signals are related through a transformation operator (wavelet propagator) that explicitly incorporates the phase and group velocities as well as the attenuation factor of the medium. In HOLSCHNEIDER *et al.* (2005a), we discuss how minimization of a cost functional based on this transformation operator allows the estimation of the dispersion properties in the case of single-mode signals. This method owes its robustness to the fact that the minimization process involves not only the modulus but also the phase of the wavelet transform, thus making it generally possible to reconstruct the dispersed signal from the manipulated wavelet coefficients. Recently, HOLSCHNEIDER *et al.* (2005b) expanded this operator using a complex-valued Cauchy

¹ Institute for Mathematics, University of Potsdam, Am Neuen Palais 10, 14469 Potsdam, Germany.
E-mail: mkulesh@math.uni-potsdam.de

² Institute for Geosciences, University of Potsdam, Karl-Liebknecht-Strasse 24–25, 14414 Potsdam, Germany.

wavelet in the case when the relationship between the phase velocity and the attenuation is satisfied by a causality constraint.

For more complex signals in which the individual modes cannot be easily separated in the time-frequency representation, a preprocessing step is required for the method proposed in HOLSCHNEIDER *et al.* (2005a). Within this step, it is necessary to define the number of propagating modes contained in the signals observed at aligned stations. For each mode, as is required for the optimization method, we need to also then specify a frequency-dependent phase velocity curve as an initial condition.

Here, we propose a solution for finding such initial guesses for the optimization problem. The wavelet propagator introduced by KULESH *et al.* (2005) demonstrates that the group velocity is a function, which “deforms” the image of the absolute value of the source signal’s wavelet spectrum. The phase velocity “deforms” the image of the wavelet spectrum phase, and the attenuation function determines the frequency-dependent real coefficient by which the spectrum is multiplied. It allows us to use the correlations between phases of the signals’ wavelet spectra to perform a “frequency-velocity” analysis in analogy to frequency-wavenumber (f - k) analysis.

Frequency-wavenumber techniques have been widely used for estimating apparent phase velocities of transient seismic phases (for a review see, e.g., ROST and THOMAS, 2002). They are also suited for deriving phase velocity curves. The following methods are the most widely utilized techniques applied in seismological applications: Conventional frequency-wavenumber method (beamformer) introduced by BURG (1964), the high-resolution f - k analysis by CAPON (1969) and the *MU*ltiple *S*ignal *C*lassification (MUSIC) method by SCHMIDT and FRANKS (1986). All of these methods usually require a substantial number of simultaneous recordings to allow for stable and reliable phase velocity estimates. In this study, we suggest a new mathematical implementation of f - k analysis based on the continuous wavelet transform and its correlations.

In general, cross-wavelet analysis of time series is not a new method. For example, the wavelet cross spectra and wavelet coherency were discussed by MARAUN *et al.* (2007). GURLEY *et al.* (2003) analyzed the time-frequency wavelet-based coherence map in light of the inherent noise in estimates. In comparison with the above-mentioned papers, the major novelty in our suggested method is the application of correlations between phases of wavelet spectra which do not contain any amplitude information.

This is especially useful for the analysis of highly dynamic time series that contain nonstationarities and have their respective signal information spread in broad frequency bands at very variable amplitude levels. These characteristics are particularly found for seismic signals to which we apply in the following our method. Here, we are especially interested in the frequency velocity analysis of transients of dispersed seismic surface waves.

The paper is organized as follows. In the first section, after the introduction and a short overview of the continuous wavelet transform method, we present our concept of wave propagation modeling in the wavelet domain with the use of a wavelet propagator. In the next section, we present the extension of a wavelet propagator to the

“frequency-velocity” analysis of multi-mode signals and demonstrate this technique with synthetic examples. Finally, using experimental data, we compared our method with the results from independent methods such as MUSIC and Capon’s spectral analysis. The last section is devoted to discussions and concluding remarks, where we note some merits of the presented approach.

2. Asymptotic Propagator In Wavelet Space

Let us assume that $S_k(t)$ and $S_m(t)$ represent two signals observed at two stations, a distance $D_{mk} = D_m - D_k$ apart. If dispersive and dissipative characteristics of the medium are represented by the frequency-dependent wavenumber $k(f)$ and attenuation coefficient $\alpha(f)$, the relation between the Fourier transforms of these signals reads

$$\hat{S}_m(f) = e^{-i\mathbb{K}(f)D_{mk} - 2\pi i n} \hat{S}_k(f), \tag{1}$$

where $n \in \mathbb{N}$ is any integer number and $\mathbb{K}(f)$ is the complex wavenumber which can be defined by real functions $k(f)$ and $\alpha(f)$ as $\mathbb{K}(f) = 2\pi k(f) - i\alpha(f)$.

Using the method fully described by KULESH *et al.* (2005), we express the spectral propagator (1) in terms of the wavelet transform of the source signal, $W_g S_k(t, f)$ and propagated signal, $W_g S_m(t, f)$.

The wavelet transform of a signal $S(t) \in L^2(\mathbb{R})$ with respect to a mother wavelet $g(t)$ is a set of L^2 -scalar products of all dilated and translated wavelets with an arbitrary signal to be analyzed (HOLSCHNEIDER, 1995):

$$W_g S(t, a) = \langle g_{t,a}, S \rangle = \int_{-\infty}^{+\infty} \frac{1}{a} g^* \left(\frac{\tau - t}{a} \right) S(\tau) d\tau, \quad a \in \mathbb{R}^+, \quad t \in \mathbb{R},$$

where $g_{t,a}(\tau) = \frac{1}{a} g((\tau - t)/a)$ is generated from a wavelet $g(\tau)$ through dilation a and translation t . The symbol $(\cdot)^*$ denotes the complex conjugate. The wavelet $g(t)$ is assumed to be a function which is well localized both in time and frequency and obeys the

oscillation condition $\int_{-\infty}^{+\infty} g(t) dt = 0$.

The wavelet transform can be expressed in terms of the Fourier transform $\hat{S}(\zeta)$ of $S(t)$ as

$$W_g S(t, a) = \int_{-\infty}^{+\infty} \hat{g}^*(a\zeta) e^{2\pi i t \zeta} \hat{S}(\zeta) d\zeta, \tag{2}$$

and the inverse of the scale $1/a$ may be associated with a frequency measured in units of the central frequency of $g(t)$. If the central frequency of the wavelet is assumed to be f_0 , each scale a can be related to the physical frequency f by $a = f_0/f$. Therefore, if we select a wavelet with a unit central frequency, it is possible to obtain the physical frequency directly by taking the inverse of the scale.

An example of the wavelet with a unit central frequency is the complex Morlet wavelet (HOLSCHNEIDER, 1995). This wavelet is convenient for the analysis of seismic signals and can be written with its Fourier transform as

$$g(t) = e^{2\pi i t} e^{-\frac{t^2}{(2\sigma^2)}}, \quad \hat{g}(\omega) = \sigma\sqrt{2\pi} e^{-\frac{\sigma^2(\omega-2\pi)^2}{2}},$$

where $\omega = 2\pi f$ is the circular frequency and parameter σ describes the variance of the wavelet. Characteristic representation of Morlet wavelet in time and frequency domain is shown in Figure 1.

From equations (1) and (2), the wavelet transform of $S_m(t)$ expressed in terms of the Fourier transform of $S_k(t)$ yields

$$\mathcal{W}_g S_m(t, f) = \int_{-\infty}^{+\infty} \hat{g}^*(\zeta/f) e^{2\pi i t \zeta} e^{-i\mathbb{K}(\zeta) D_{mk} - 2\pi i n \hat{S}_k(\zeta)} d\zeta.$$

Let us assume that frequency-dependent wavenumber and attenuation are slowly varying with regard to the frequency range of the mother wavelet. For moderate dispersion, the complex wavenumber can be approximated by the first two terms of its Taylor series around the frequency f : $\mathbb{K}(\zeta) = \mathbb{K}(f) + (\zeta - f)\mathbb{K}'(f) + O(|\zeta - f|^2)$. Upon inserting this approximation into the integral above, we obtain

$$\mathcal{W}_g S_m(t, f) = e^{-i[\mathbb{K}(f) - f\mathbb{K}'(f)] D_{mk} - 2\pi i n} \int_{-\infty}^{+\infty} \hat{g}^*(\zeta/f) e^{2\pi i [t - \mathbb{K}'(f) D_{mk} / (2\pi)] \zeta} \hat{S}_k(\zeta) d\zeta. \quad (3)$$

There are two different ways to calculate the integral in equation (3). Following the first way, a special wavelet-like Cauchy wavelet can be used, which can absorb the imaginary part of the time shift concerned with the attenuation. As a result, we obtain an asymptotic

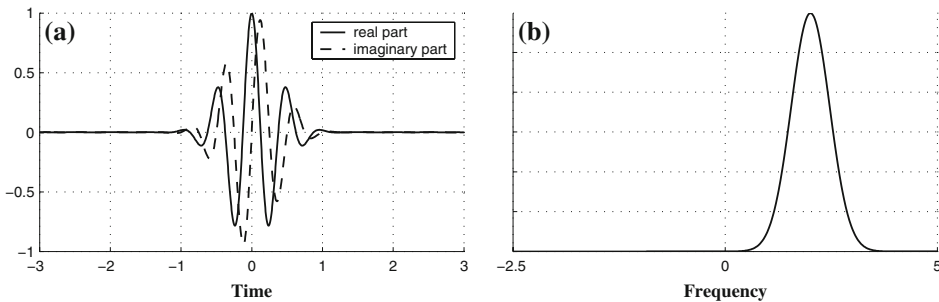


Figure 1

Representation of Morlet wavelet in (a) time and (b) frequency domain, $\sigma = 1/2$. Wavelet is progressive and has the unit central frequency.

propagator in wavelet space in the case where the relationship between the phase velocity and the attenuation is satisfied by a causality constraint (HOLSCHNEIDER *et al.*, 2005b).

Instead of the use of special wavelets, we can also use another approximation that is useful in seismology – so called “constant Q attenuation” approach or frequency – independent attenuation. This behavior is a result of the multitude of seismic attenuation mechanisms present in the earth, each of which having some frequency dependence, but together producing a form of attenuation when the attenuation quality parameter $Q = \pi f / (C_p(f)\alpha)$ is constant (KJARTANSSON, 1979; TURNER and SIGGINS, 1994). In such a case, if the phase velocity $C_p(f)$ is nearly linear, then $\alpha'(f) \approx 0$ and the asymptotic propagator in the wavelet space has the form (KULESH *et al.*, 2005):

$$\mathcal{W}_g S_m(t, f) = e^{-\alpha D_{mk}} e^{-2\pi i [k(f) - f k'(f)] D_{mk} - 2\pi i n} \mathcal{W}_g S_k(t - k'(f) D_{mk}, f). \quad (4)$$

In the special case, with the assumption that the analyzing wavelet has a linear phase (with time-derivative approximately equal to 2π as is the case for the Morlet wavelet), the approximation can be written in terms of the phase $C_p(f)$ and group $C_g(f)$ velocities as:

$$\mathcal{W}_g S_m(t, f) = e^{-\alpha D_{mk}} \left| \mathcal{W}_g S_k \left(t - \frac{D_{mk}}{C_g(f)}, f \right) \right| \exp \left[i \arg \mathcal{W}_g S_k \left(t - \frac{D_{mk}}{C_p(f)} - \frac{n}{f}, f \right) \right], \quad (5)$$

where

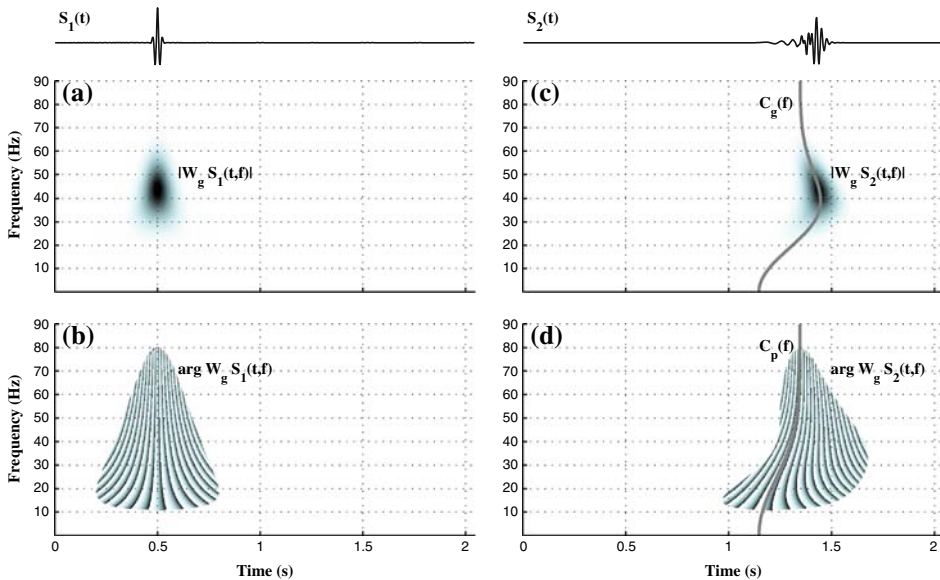


Figure 2

Propagated synthetic signal and its wavelet transform: (a),(c) are the power (absolute value squared) of the wavelet coefficients and (b),(d) are the corresponding phase images. The lines in (c) and (d) show frequency-dependent group and phase velocities used in propagation model.

$$C_p(f) = \frac{f}{k(f)}, \quad C_g(f) = \frac{1}{k'(f)} = \frac{C_p^2(f)}{C_p(f) - fC_p'(f)}. \quad (6)$$

The relationship (5) has the following interpretation: The group velocity is a function that “deforms” the image of the absolute value of the source signal’s wavelet spectrum, the phase velocity “deforms” the image of the wavelet spectrum phase, and the attenuation function determines the frequency-dependent real coefficient by which the spectrum is multiplied.

This behavior is demonstrated in Figure 2, where we consider a synthetic signal $S_1(t)$. In this example, we use a propagation phase and group velocities, which are not based on a physical model. These frequency-dependent velocities are shown in Figures 2c,d. We perform the propagation of signal $S_1(t)$ using equation (1) and obtain a propagated counterpart $S_2(t)$. The gray-scaled images in Figure 2 show the absolute values and phases of wavelet spectra $\mathcal{W}_g S_1(t, f)$ and $\mathcal{W}_g S_2(t, f)$. We see that the deformations of images labeled as $|\mathcal{W}_g S_2(t, f)|$ and $\arg \mathcal{W}_g S_2(t, f)$ agree in general with velocities curves $C_g(f)$ and $C_p(f)$ accordingly, but have small distinctions that demonstrate the asymptotic properties of the equation (5).

3. Wavelet Based Frequency-velocity Analysis

The equation (5) and Figure 2 allow us to formulate an idea as to how the frequency-dependent phase velocity can be obtained using the wavelet spectra’ phases of source and propagated signals. Using the correlations between two spectra, we can perform “frequency-velocity” analysis on the analogy of the frequency-wavenumber method (CAPON, 1969) for a seismogram $S_k(t)$, $k = 1, \dots, N$. The main part of this analysis constitutes in the calculation of correlation spectrum $\mathbf{M}(f, c)$ as follows:

$$\begin{aligned} \mathbf{M}(f, c) &= \int_{t_{\min}}^{t_{\max}} \left| \sum_{k,m} \Phi_k(\tau, f) \Phi_m^*(\tau - D_{mk}/c, f) \right| d\tau \\ &= \int_{t_{\min}}^{t_{\max}} \left| \sum_{k,m} \exp(i\Psi_k(\tau, f)) \exp(-i\Psi_m(\tau - D_{mk}/c, f)) \right| d\tau, \end{aligned} \quad (7)$$

where $[t_{\min}, t_{\max}]$ indicate the total time range for which the wavelet spectrum was calculated, $c \in [C_p^{\min}, C_p^{\max}]$ is an unbound variable corresponding to the phase velocity, Φ_k is a complex-valued wavelet phase, Ψ_k is a real-valued wavelet phase and D_{mk} is the distance between two stations indexed k and m .

Correlation spectrum $\mathbf{M}(f, c)$ is calculated using only the correlations between phases of wavelet spectra; these phases contain no amplitude information. Using this fact, we can adopt an alternative definition of a multi-trace correlation expression:

$$\mathbf{M}(f, c) = \int_{t_{\min}}^{t_{\max}} \left| \prod_{k=1}^N \Psi_k(\tau - D_{1k}/c, f) \right| d\tau. \tag{8}$$

The wavelet phases $\Phi_k(\tau, f)$ and $\Psi_k(\tau, f)$ in equations (7) and (8) are defined as

$$\Phi_k(\tau, f) = \frac{W_g S_k(\tau, f)}{|W_g S_k(\tau, f)|}, \quad \Psi_k(\tau, f) = \arg W_g S_k(\tau, f). \tag{9}$$

To decrease the influence of low-amplitude noise in source signal on the correlation spectrum $\mathbf{M}(f, c)$, we can consider a threshold operation based on the amplitude of wavelet coefficients instead of total phases defined in equation (9). For example, such a threshold operation for real-valued wavelet phase can be introduced as

$$\Psi_\varepsilon(\tau, f) = \begin{cases} \Psi(\tau, f) & \text{if } |W_g S(\tau, f)| > \varepsilon, \\ 0 & \text{otherwise.} \end{cases} \tag{10}$$

To obtain the phase velocities, we plot $\mathbf{M}(f, c)$ as a surface on “frequency” and “velocity” axes. The local maxima in this surface correspond to phase velocities of the propagating modes within the medium and observed in the seismograms. To improve the contrast of such scalograms for the purpose of visualization, instead of $\mathbf{M}(f, c)$ we can plot a power function of the normalized correlation coefficients as

$$\mathbf{M}_p(f, c) = \left(\frac{\mathbf{M}(f, c)}{\max_{c \in [C_p^{\min}, C_p^{\max}]} \mathbf{M}(f, c)} \right)^p, \tag{11}$$

where we consider the maximum of correlation spectrum $\mathbf{M}(f, c)$ over velocity $c \in [C_p^{\min}, C_p^{\max}]$ for each frequency separately.

To demonstrate this concept, a synthetic seismogram with two modes with different wave numbers but with the same frequency content is analyzed. We consider the situation without attenuation: $\alpha = 0$:

$$\hat{S}_m(f) = e^{-2\pi i k_1(f) D_{m1}} \hat{S}_k(f) + e^{-2\pi i k_2(f) D_{m2}} \hat{S}_k(f) \tag{12}$$

Given two different phase velocities, from which the wavenumbers are computed, a propagation modeling was performed using equation (1); the synthetic traces are formed then by adding the pulses obtained from the inverse Fourier transform of equation (1). In this manner, seven seismic traces were generated to simulate the observation at seven successive stations. These traces are presented in Figure 3a. The phase velocities used for this seismogram generation are plotted in Figures 3b,c as solid curves; fundamentally this condition describes first symmetric and asymmetric modes of Lamb wave.

We perform the “frequency-velocity” analysis of this synthetic seismogram using both equations (7) and (8) with a threshold operation given in equation (10) where $\varepsilon = 0.1\%$ of the maximum modulus of the wavelet transform. Then we plot the power

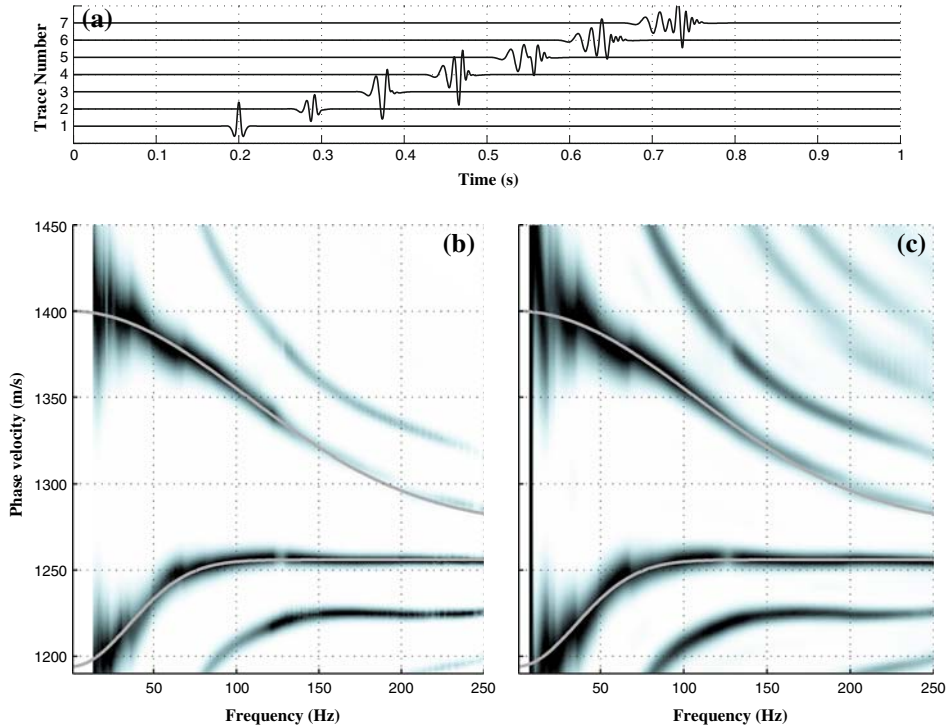


Figure 3

Frequency-velocity analysis of seismic arrivals that consist of two interfering pulses of different dispersion characteristics: (a) The synthetic seismogram, correlation spectrum using (b) real-valued wavelet phases and (c) complex-valued phases.

function of normalized correlation coefficients introduced by equation (11) with $p = 1$. The greyscale background image in Figure 3b shows the result of the correlation between real-valued wavelet phases using equation (8), and Figure 3c shows the correlation result when using complex-valued phases and equation (7). The agreement of the correlation coefficients' maximum lines with theoretical phase velocities is very good in both methods.

Four extra "pseudomodes" presented in Figures 3b,c are justified on the basis of 2π -cycle skips between the stations introduced in equation (1) and remaining in the wavelet propagator (5) as n/f item. These "pseudomodes" can be filtered by analyzing the group velocities obtained from the maximum lines of the correlation image with the help of equations (6).

Both methods (7) and (8) have two tuning parameters, such as the parameter of the wavelet σ and threshold of phase sensitivity ε . The felicitous choice of these parameters is important for the successful processing. To demonstrate it, we extract from the calculation procedure (8) some intermediate data and show it in Figure 4. The panel (a)

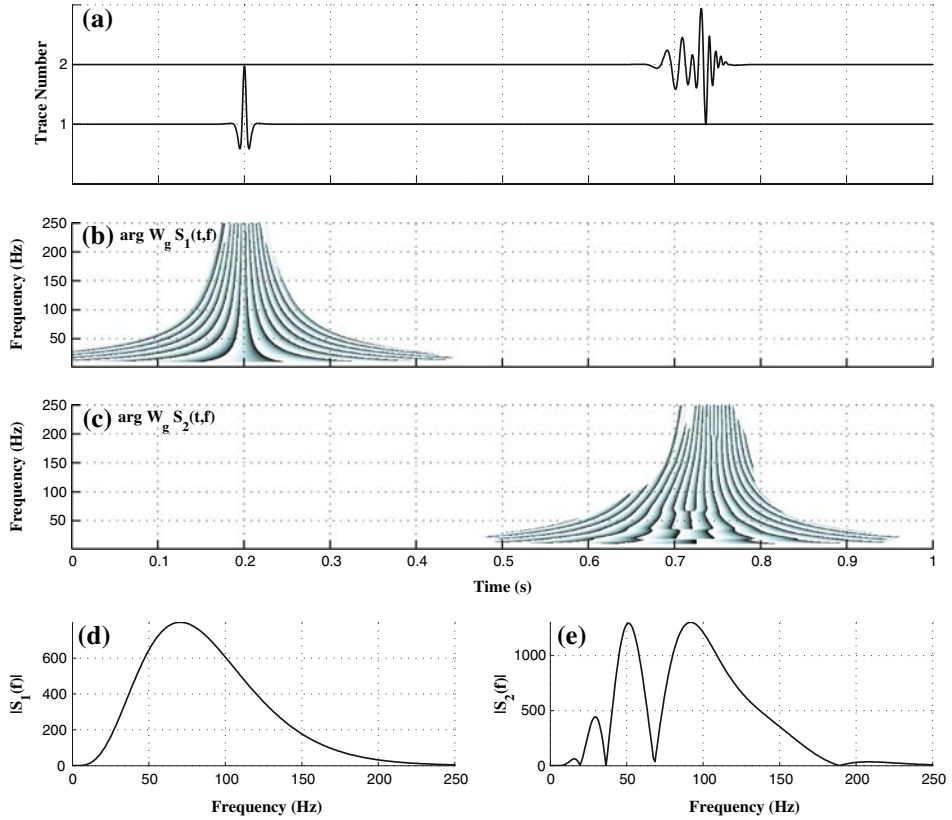


Figure 4

Time-frequency representation of two signals used in the frequency-velocity analysis in Figure 3: (a) Two analyzed signals, (b),(c) real-valued phases $\Psi_k(t, f)$ and (d),(e) Fourier spectra of these signals.

of this figure contains two traces from Figure 3a—the first $S_1(t)$ and the last $S_2(t)$. The Fourier spectrum of these signals is shown in Figures 4d,e. To show the time-frequency content of these signals, we save the wavelet phases $\Psi_k(t, f)$ at the time of calculation. After applying the threshold operation (10) with $\varepsilon = 0.1\%$ of maximum modulus of wavelet transform, we plot these phases in Figures 4b,c.

The wavelet parameter σ defines the width of the phases structures labeled as $\arg \mathcal{W}_g S_1(t, f)$ and $\arg \mathcal{W}_g S_2(t, f)$ in Figures 4b,c; with the increase of this parameter we improve the time resolution and consequently the accuracy of the correlation coefficients in the middle frequency band. However, in this case, we lose the precision in the lowest and highest frequency ranges. Furthermore, we need longer time representation of the wavelet spectrum, because a time cut-off (as we have at the beginning of the spectrum $\arg \mathcal{W}_g S_1(t, f)$ between 5 and 30 Hz) can cause the numerical error in the corresponding frequency band. The parameter ε defines the low-frequency cut-off that causes the white

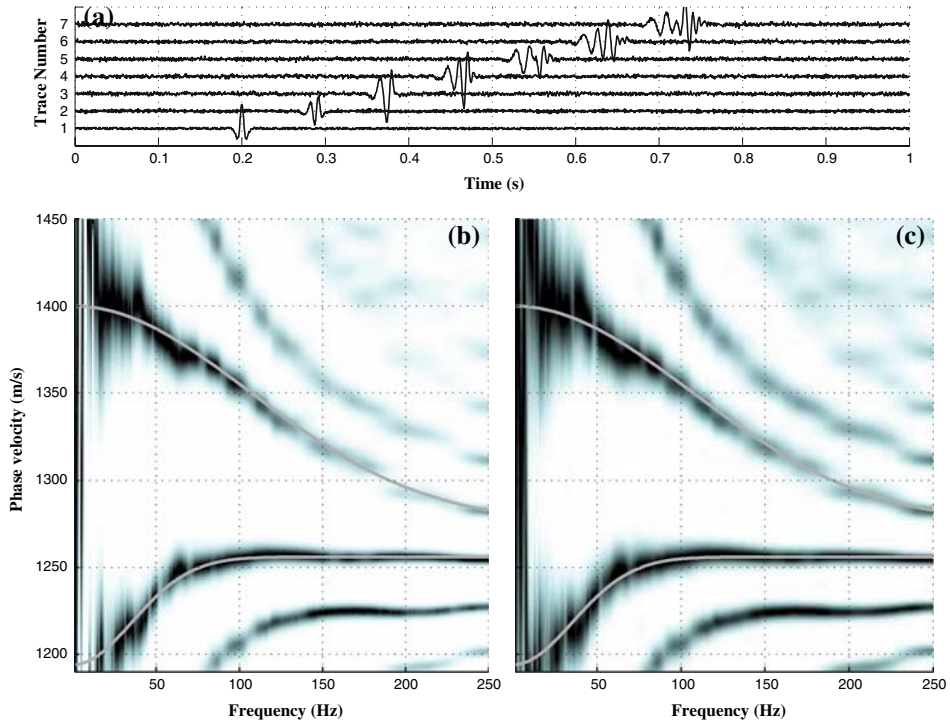


Figure 5

Frequency-velocity analysis of noised seismic arrivals with two interfering pulses.

vertical regions in Figures 3b,c for frequencies less than 10 Hz. With the increase of this parameter we miniaturize the phase areas to the time-frequency regions with greater amplitudes and, therefore, we reduce the influence on the low-amplitude noise.

In order to demonstrate the noise stability of this method, we perform the “frequency-velocity” for the same example but add random noise to the source signal. The noise level is about 5% related to the peak-to-peak amplitude of the original signal presented in Figure 3a. These noisy seismograms are plotted in Figure 5a; Figures 5b,c show the correlation images using methods (8) and (7) accordingly. From this example, we can conclude that the noise stability of the presented approach is sufficiently high for the successful analysis of signals disturbed by additive uncorrelated noise.

4. Application to Experimental Data

In this section we use the field data to verify the ability of the proposed method to estimate phase velocities. We previously analyzed these data in (HOLSCHNEIDER *et al.*

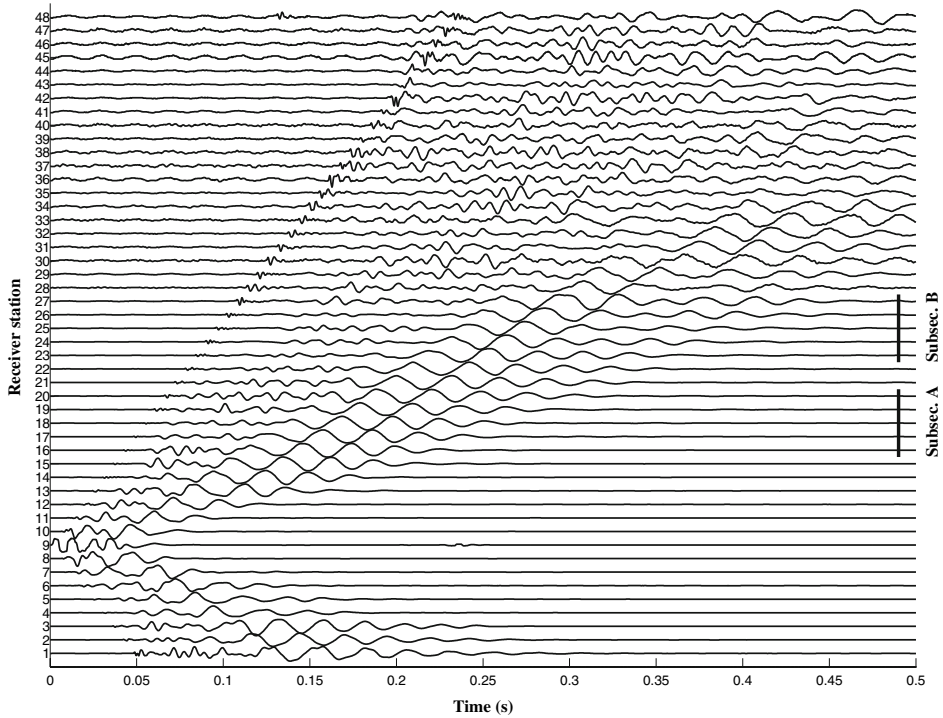


Figure 6

Observed seismograms obtained from a shallow seismic experiment using a sledgehammer as a source. The distance between consecutive stations is 2 m.

(2005a) where we successfully estimated the phase and group velocities as well as attenuation using a minimization procedure for the inversion of equation (5). Here we utilize this equation again in order to introduce the correlation computation given in equation (8).

The experimental data set shown in Figure 6 consists of a 2-D shallow seismic survey (stations along a line) at Kerpen, a particular site in the Lower Rhine embayment where the buried scarp of a historically active fault is presumed. Presented vertical displacement for 48 channels with 2 m inter-receiver spacing were collected using hammer blows as seismic source. We selected a seismogram profile with prominent low frequency, high amplitude arrivals that correspond to the surface wave arrivals we intend to characterize.

We selected two subsections from the seismograms for our analysis. These subsections are labeled “subsection A” and “subsection B” in Figure 6. For each subsection, we perform the “frequency-velocity” analysis with the use of correlation between real-valued wavelet phases using equation (8) with a threshold operation given in equation (10) where $\varepsilon = 0.1\%$ of maximum modulus of wavelet transform. We present

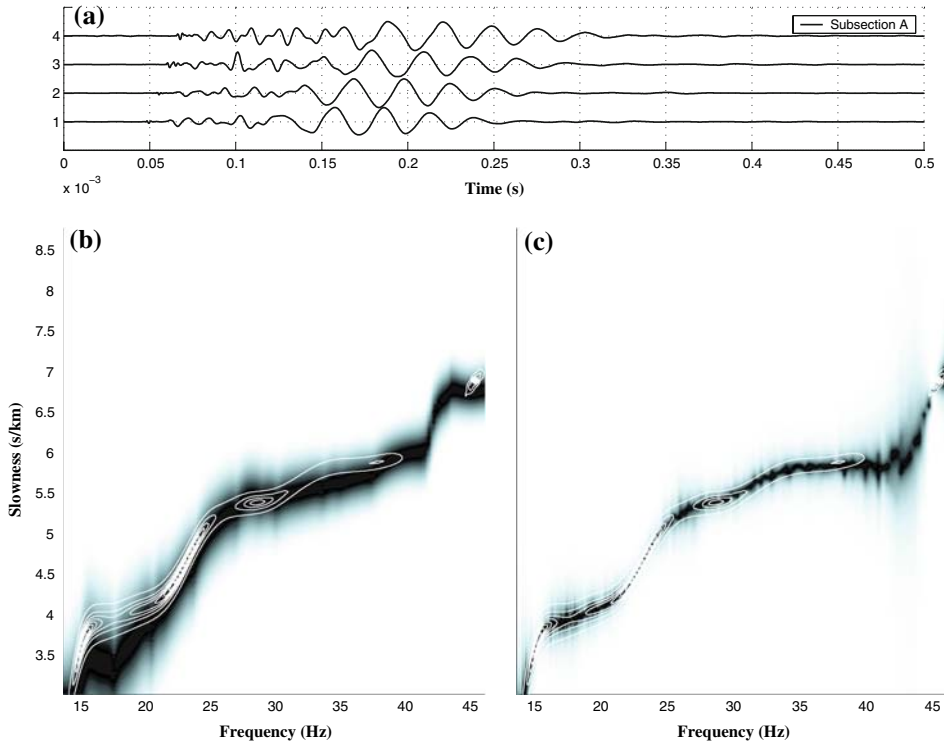


Figure 7

The “frequency-velocity” analysis of subsection A.

the results of this analysis for two subsections in Figures 7b and 8b as greyscale background image, where we plot the slowness $s(f) = 1 / C_p(f)$.

To check the quality of our correlation method, we evaluated the slowness using two alternative methods as described in HOLSCHNEIDER *et al.* (2005a):

- **CAPON** high-resolution method (CAPON, 1969). An estimate of the phase velocity $C_p(f)$ of a plane wave front recorded by N sensors at position vectors \mathbf{r}_k by Capon’s algorithm is obtained by maximizing the expression

$$P(f, \mathbf{k}) = \frac{1}{\mathbf{A}^T(f, \mathbf{k})\mathbf{R}^{-1}(f)\mathbf{A}(f, \mathbf{k})}, \tag{13}$$

where $\mathbf{A}(f, \mathbf{k})$ are the steering vectors accounting for the travel–time delays of the plane front with components $\alpha_k(f, \mathbf{k}) = e^{i\mathbf{k}^{(f)} \cdot \mathbf{r}_k}$, $k = 1, \dots, N$. The vector $\mathbf{k}(f)$ denotes the horizontal wavenumber vector with $|\mathbf{k}| = f / C_p(f)$ and the direction of arrival is given by $\beta = \arctan(k_y / k_x)$. $\mathbf{R}(f)$ is a cross–spectral matrix formed from the pairwise cross spectra of the signals $S(\mathbf{r}_k, t)$ as

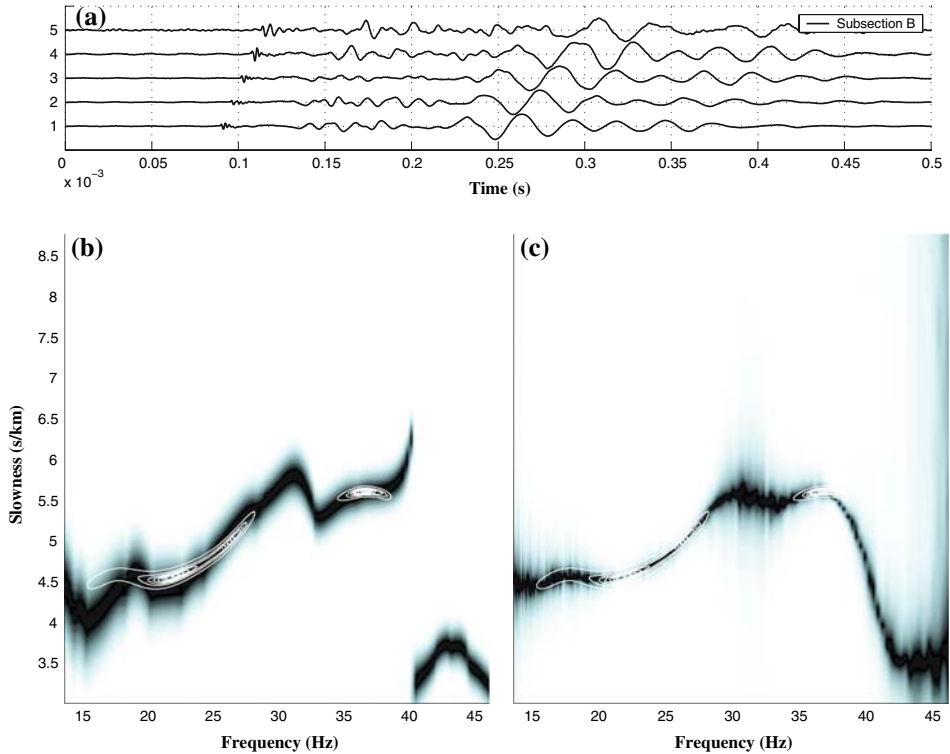


Figure 8
The “frequency-velocity” analysis of subsection B.

$$\mathbf{R}(f) = \begin{bmatrix} \hat{S}(\mathbf{r}_1, f)\hat{S}^*(\mathbf{r}_1, f) & \cdots & \hat{S}(\mathbf{r}_1, f)\hat{S}^*(\mathbf{r}_N, f) \\ \vdots & \ddots & \vdots \\ \hat{S}(\mathbf{r}_N, f)\hat{S}^*(\mathbf{r}_1, f) & \cdots & \hat{S}(\mathbf{r}_N, f)\hat{S}^*(\mathbf{r}_N, f) \end{bmatrix}$$

For the linear receiver configuration of the hammer shot dataset, we perform the maximization of equation (13) in a grid search manner along the one-dimensional wavenumber grid projected along the source-receiver direction.

- **MUSIC** high-resolution method (SCHMIDT and FRANKS, 1986). This method belongs to the class of subspace methods. Those methods rely on the orthogonality between signal and noise subspaces spanned by the eigenvectors of the cross-spectral matrix $\mathbf{R}(f)$ to deduce signal propagation characteristics for multiple signal contributions. The phase velocities of multiple sources (arrivals) can be derived by searching for the roots of the signal steering vectors projected onto the noise subspace or equivalently by maximizing the function

$$P(f, \mathbf{k}) = \left(\sum_{k=q+1}^N |\mathbf{A}^T(f, \mathbf{k}) \cdot \mathbf{E}_k(f)|^2 \right)^{-1}, \quad (14)$$

where $\mathbf{E}_k(f)$, $k = 1, \dots, N$ are the normalized eigenvectors of $\mathbf{R}(f)$, q denotes the number of acting sources and $\mathbf{A}(f, \mathbf{k})$ are the steering vectors as above. The maximization of equation (14) is performed again by a grid search approach and the number of sources q is estimated by an information theoretical approach (WAX and KAILATH, 1985) based on Akaike's criterion (AKAIKE, 1973).

We selected the complete waveform windows of subarrays corresponding to subsections A and B along the shot profile to compute $P(f)$ in equations (13) and (14) for horizontal wavenumbers k sampled equidistantly in one dimension, and for a set of 200 discrete frequencies spaced equidistantly on a logarithmic frequency scale from 10 to 50 Hz. In Figures 7c and 8c, we display the results of this analysis for two subarrays. Each subfigure displays the results of the MUSIC approach as a greyscale background image. For better visibility we normalized the maxima to one for each individual analysis frequency. The greyscale background depicting the result from the MUSIC approach shows a decreased resolution of the velocity in the frequency range where the surface wave is highly attenuated, indicated by the peak broadening along the vertical scale.

The superimposed contour lines delineate the distribution of $P(f)$ from Capon's analysis method. It is interesting to note that the contour plot of Capon's analysis results does not reach the frequency range from which the surface wave is highly attenuated.

The region where the phase velocity estimates from all methods come quite close corresponds to those in which the energy of the surface arrival is significantly high (around 20 Hz and 30 Hz). The relatively large misfit between the velocity estimates from the presented method and those from MUSIC and Capon's analysis is probably due to the sensitivity of the methods to the reduced signal-to-noise ratio in this frequency range. A second possible cause for this misfit may be the approximation base of the wavelet propagator (5). In spite of this misfit, we can establish a good agreement between all considered methods.

5. Conclusions and Discussion

In this study we extended the wavelet propagator proposed in our previous work to the method of "frequency-velocity" analysis in analogy to the classical frequency-wavenumber ($f-k$) analysis methods. The wavelet propagator is a mathematical model for establishing a link between the continuous wavelet transform of a signal and its propagated counterpart in a dispersive and attenuating medium. From this property, we perform the "frequency-velocity" analysis using correlation calculations between phases of signals' wavelet spectra.

The “frequency-velocity” analysis is an approximate approach and therefore there is some misfit between the velocity estimates from the presented method on one hand and those from another high-resolution f - k methods on the other. We demonstrate it by the analysis of experimental field data.

Note that the wavelet propagator (5) contains both phase and group velocities as parameters. At first sight, the correlation calculations between absolute values of the signals’ wavelet spectra seem to be useful for obtaining the group velocities. However, the numerical simulations show that the correlation of absolute values is very sensible to noise and therefore is not effective when applied to real data.

From analysis of synthetic and real data, we can note some merits of our approach as compared with other methods:

- Our method has two tuning parameters, such as the parameter of the wavelet σ and threshold of phase sensitivity ε . These two parameters allow us to vary the sensitivity of method in compliance with considered signals.
- The method has no constraints as to the number of analyzed traces in a seismogram; it is possible to use only two or three traces.
- The determination of several mode branches is feasible.

Acknowledgements

This project is supported by a grant from the Deutsche Forschungsgemeinschaft (DFG) within the framework of the priority program SPP 1114 “Mathematical methods for time series analysis and digital image processing.”

REFERENCES

- AKAIKE, H. (1973), *Information theory and an extension of the maximum likelihood principle*, 2nd Interna. Symp. on Information Theory, pp. 267–281.
- BURG, J. P. (1964), *Three-dimensional filtering with an array of seismometers*, *Geophysics* 29(5), 693–713.
- CAPON, J. (1969), *High-resolution frequency-wavenumber spectrum analysis*, *Proc IEEE* 57(8), 1408–1418.
- GURLEY, K., KIJEWski, T., and KAREEM, A. (2003), *First-and higher-order correlation detection using wavelet transforms*, *J. Engin. Mechanics* 129(2), 188–201.
- HOLSCHNEIDER, M. (1995), *Wavelets: An Analysis Tool*. (Oxford: Clarendon Press, 1995).
- HOLSCHNEIDER, M., DIALLO, M. S., KULESH, M., OHRNBERGER, M., LÜCK, E., and SCHERBAUM, F. (2005a), *Characterization of dispersive surface waves using continuous wavelet transforms*, *Geophys. J. Internat.* 163(2), 463–478.
- HOLSCHNEIDER, M., KULESH, M., DIALLO, M. S., KURENNAYA, K., and SCHERBAUM, F., (2005), *Modeling of wave dispersion using continuous wavelet transforms: incorporating causality constraint with non-linear frequency-dependent attenuation*, *EOS Trans. AGU*, 86(52), Fall Meet. Suppl., Abstract S33A–0289.
- KJARTANSSON, E. (1979), *Constant Q-wave propagation and attenuation*, *J. Geophys Res* 84(B9), 4737–4748.
- KULESH, M., HOLSCHNEIDER, M., DIALLO, M. S., XIE, Q., and SCHERBAUM, F. (2005), *Modeling of wave dispersion using continuous wavelet transforms*, *Pure App.Geophys.* 162(5), 843–855.

- MARAUN, D., KURTHS, J., and HOLSCHNEIDER, M. (2007), Nonstationary Gaussian processes in wavelet domain: Synthesis, estimation, and significance testing, *Phys. Rev. E (Statistical, Nonlinear, and Soft Matter Physics)*, 75(1), 016707.
- ROST, S. and THOMAS, C. (2002), *Array seismology: methods and applications*, *Rev. Geophys.* 40(3), 2–1 – 2–27.
- SCHMIDT, R. and FRANKS, R. (1986), *Multiple source DF signal processing: An experimental system*, *Antennas and Propagation*, IEEE Transactions 34(3), 281–290.
- TURNER, G. and SIGGINS, A. F. (1994), *Constant Q attenuation of subsurface radar pulses*, *Geophysics*, 59(8), 1192–1200.
- WAX, M. and KAILATH, T. (1985), *Detection of signals by information theoretic criteria*, IEEE Transactions on ASSP, 33(2), 387–392.

(Received January 10, 2007, accepted August 7, 2007)

Published Online First: February 28, 2008

To access this journal online:
www.birkhauser.ch/pageoph
